Preloading of four-legged jack-ups in clay
Geotechnical time effects and fulfilment of preloading criteria

Sonnema, Wouter; Brinkman, Sanne; Brinkgreve, Ronald B.J.; Pisano, Federico

Important note
To cite this publication, please use the final published version (if applicable).
Please check the document version above.

Preloading of four-legged jack-ups in clay: Geotechnical time effects and fulfilment of preloading criteria

Wouter Sonnema [a], Sanne Brinkman [b], Ronald B.J. Brinkgreve [c], Federico Pisanò [c,*]

[a] *Heerema Marine Contractors, Vondellaan 47, Leiden, 2332 AA, The Netherlands*
[b] *Van Oord, Schaardijk 211, Rotterdam, 3063 NH, The Netherlands*
[c] *Faculty of Civil Engineering and Geosciences, Delft University of Technology, Stevinweg 1, Delft, 2628 CN, The Netherlands*

ARTICLE INFO

ABSTRACT

Presented here is a numerical study on the preloading of four-legged jack-ups, such as those commonly employed in the construction of offshore wind farms. The need for reducing jack-up installation time is particularly felt within the offshore industry, especially when multiple preloading cycles are necessary in clayey soils to fulfil given preloading criteria. This is due to clays experiencing delayed deformations, causing load redistribution among all legs while the ideal situation of steady preload on all spudcans is pursued. This work employs three-dimensional finite element (3D FE) modelling to analyse the preloading performance of a reference jack-up vessel in clayey soils using a wished-in-place (WIP) approach. Detailed modelling of time effects due to soil consolidation and viscosity is introduced, with some emphasis on how to derive material parameters from typical site investigation and laboratory soil data. The results of specific parametric studies are presented to support the suitability of the adopted analysis approach, also with regard to the adoption of alternative preloading procedures. The constitutive modelling of time-dependent clay's behaviour is shown to play a crucial role in the considered framework, and will require further research for 3D FE modelling to provide reliable quantitative support to real wind farm installation projects.

1. Introduction

Mobile jack-up platforms have been used in the offshore industry for a long time, originally in relation to oil and gas drilling activities. Jack-ups used in that context would usually comprise a triangular hull supported by three retractable legs, fitted with so-called *spudcans* – saucer-shaped polygonal footings with a central spigot and sloping conical underside (Dean, 2010; Randolph and Gourvenec, 2011). More recently, the booming offshore wind industry has been relying on jack-up vessels equipped with more than three legs (four or six). Owing to their self-installing and self-elevating capabilities, they are perfectly suited for installation and maintenance activities at new or existing offshore wind farms (Fig. 1) (Globaldata, 2012). Four/six-legged jack-ups usually feature steel legs that are either tubular or trussed: tubular legs are easier to construct and typically require less space on and below deck; conversely, trussed legs are typically lighter (lower use of steel) and more effective in reducing drag loads when operating in deeper waters. To accommodate the increasing size of wind turbine structures, the dimensions of jack-up legs and hulls have also been growing – respectively, beyond 125 m (Welaya et al., 2015) and

100 m (Jiang, 2021). Such a growth has also led to the use of larger spudcan foundations, whose diameter may often range from 10 to 15 m.

The use of any jack-up requires site-specific assessment for each location where the vessel will be deployed, in order to guarantee safe installation and operations. In the last decades, significant efforts have been spent to standardise Site Specific Assessment procedures, with special attention paid to geotechnical aspects (InSafeJIP, 2011). The main outcomes of such efforts are today collected in the ISO 19905-1 document (ISO, 2016; Hoyle et al., 2006), built on the earlier SNAME 5-5 A guidelines (SNAME, 2008). Soil–structure interaction matters dominate existing knowledge about jack-up assessment, whose understanding and application demand close collaboration between structural and geotechnical specialists (Houlsby, 2016).

As offshore wind farms are formed by numerous turbines, jack-ups are operated through multiple elevating-lowering cycles. In particular, the elevating process includes a preloading stage that enhances the geotechnical capacity of all spudcans. In the case of four-legged jack-ups, preloading is performed by alternately applying vertical loads on

Fig. 1. Aeolus offshore wind turbine installation vessel (courtesy of Van Oord).

diagonally opposite leg pairs, up to achieving a stable condition in which each leg holds nearly constant vertical load (Versteele et al., 2017). Among all possible seabed conditions a general distinction can be made between cohesive/clayey and cohesionless/sandy soils. While the latter usually imply firm seabed and minimal spudcan penetration during preloading (for instance, in North Sea dense sand), lower bearing capacity in cohesive soils can result in large penetration – possibly as large as several times the spudcan diameter. Preloading in clay is additionally complex due to the interplay of time effects stemming from consolidation (Barbosa-Cruz, 2007; Bienen and Cassidy, 2013; Stanier et al., 2014; Bienen et al., 2015; Wang and Bienen, 2016; Ragni et al., 2016, 2017) and viscous behaviour (Einav and Randolph, 2005; Andersen, 2015; Engin et al., 2019) – such interplay is also discussed in a different context by Brinkgreve (2004). In what follows, the term 'soil viscosity' is used to unify different features of time-dependent behaviour, including creep, relaxation and, sensitivity to loading rate. Spudcan settlement in consolidating/viscous soil induce in time load redistribution among different legs, and therefore longer duration of the jacking procedure. It is therefore difficult to predict accurately the total preloading time, which is key to early-stage estimations of project duration and costs. Better grasp of clay-spudcan interaction and load redistribution can positively impact the site-specific analysis of jack-up preloading, and the accuracy of related cost scenarios.

This work confirms how 3D FE modelling can well serve the integrated analysis of jack-up's behaviour (Pisanò et al., 2019), particularly in the presence of non-linear, time-dependent soil–spudcan interaction. Since a complete large-deformation analysis of jack-up installation prior to preloading was beyond the scope of this study, the simpler wished-in-place (WIP) approach was followed to reduce the complexity and computational cost of all numerical simulations. The main goal of this paper is to explore the impact of dominant geotechnical factors on the timing of jack-up preloading in clayey seabeds. Such factors include the time effects that are associated with soil consolidation and viscous behaviour, with significant role played by the geological/loading history of the seabed (over-consolidation). After a detailed description of the main model set-up/calibration steps, the developed 3D FE jack-up-soil model is finally used to compare different preloading procedures and identify opportunities for optimisation.

2. Preloading of four-legged jack-ups in cohesive soils

The preloading of four-legged jack-ups in cohesive soils is usually associated with load distribution between diagonally-opposite leg pairs, which are loaded alternately in stages of leg extension (*active preloading*). As legs are extended, additional penetration is observed. Fig. 2 exemplifies the execution of a typical preloading procedure in clayey

seabed. Prior to preloading, initial penetration of the four legs into the seabed is allowed by applying moderate loads. Preloading is then started by extending the purple legs in Fig. 2(a) – in small increments, for the sake of safety (the purple leg pair is the first to act as *active pair*, turning later into *passive pair* as the other two legs become active (Fig. 2(a))). During phases of no further extension, a decrease in vertical load is observed in the active pair due to delayed soil settlement, which is promoted by consolidation and viscous behaviour (Versteele et al., 2017). Load redistribution among the four legs is continuous and simultaneous: as the load in the active pair decreases, the opposite occurs in the passive pair. After preloading the first (purple) leg pair, the second (yellow) pair is preloaded following the same procedure. The preloading procedure is overall completed after actively loading both leg pairs. At that point, all legs will have been proven to provide a stable foundation for the jack-up up to the applied level of preloading. A higher level may be achieved by reducing the draft, i.e., by increasing the available reaction force for each leg and then repeating the same preloading procedure.

The draft of the hull during preloading depends on the targeted preload. Initially, after contact with the seabed, all four legs are extended until a load of approximately half the preload is applied to the legs, which corresponds with a draft of a few meters. The diagonal preloading is then initiated at this draft. Subsequently, the draft is reduced to enable the application of larger preloads. The final preload level that is required to withstand storm and operational conditions is determined as part of the Site Specific Assessment. In order to achieve the calculated preload it is often required to reduce the draft to low levels (1 m or less). A final preload cycle is normally executed with the hull in the air. At variance with the simplified representation in Fig. 2, uneven self-weight penetration of the legs is a quite common (and not concerning) occurrence, typically due to inhomogeneous soil conditions and structural asymmetry (the centre of gravity is not exactly at the geometrical centre of the vessel).

There are several jacking systems available on the market, such as:

- the pin and cylinder system, in which the platform is elevated or lowered by large hydraulic cylinders. When, at the end of the stroke, the leg is locked off with pins, the cylinder is reset for the next stroke. In its elevated configuration, the platform is normally supported by the pins. Unless a double set of cylinders is used, the pin and cylinder system does not enable continuous jacking, and the jacking speed is relatively low;
- the rack and pinion system. In this case the legs are provided with heavy racks which are engaged by large slow turning pinions. These large pinions are driven through a multitude of gear reductions by an electric (or hydraulic) motor. The jacking systems can be attached to the platform rigidly or with some sort of flexible support. The electric or hydraulic motor is normally provided with a fail-safe spring loaded brake system, that engages automatically when current is interrupted or hydraulic pressure drops below a certain value. During operating and storm conditions the platform is normally supported by the brake system or specific lock-off devices.

Either system is well capable of dealing with differences in leg penetration, as each leg may be extended individually. This also allows the hull to be kept approximately level during the penetration of the legs. Rack Phase Difference is a measurable difference in the vertical position of the chords relative to each other within the same leg, for the rack and pinion system. This can be the result of uneven loading of the leg chords when the spudcan is eccentrically supported.

Jack-up preloading typically includes several load cycles, which are executed to assure that each leg can withstand the preload without excessive settlement – although with the consequence of increasing the duration of the preloading phase and, therefore, the total time for wind farm installation. Empirical criteria are normally used in practice to determine whether sufficient stability/safety has been achieved or
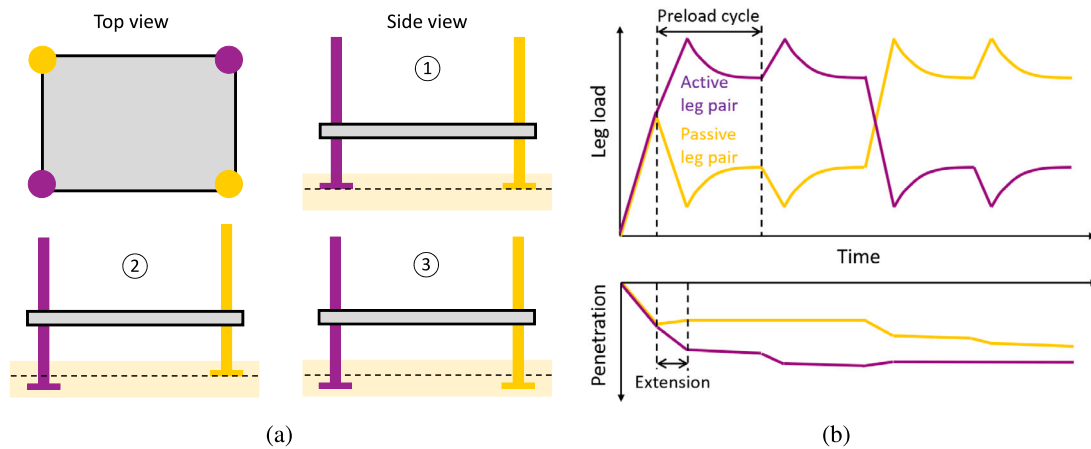
Fig. 2. Preloading procedure for four-legged jack-ups, (**a**) top and side views of the jack-up; (**b**) evolution of (normalised) leg load and penetration during preloading.
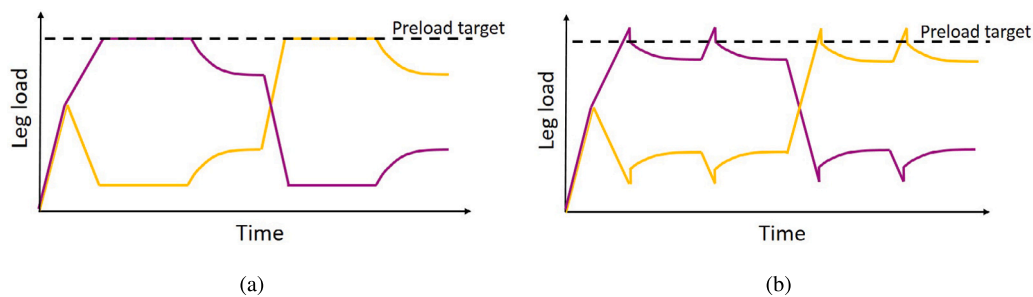

Fig. 3. Two alternative preloading procedures based on the concepts of (**a**) overshooting and (**b**) load-holding.

additional load cycles are needed. Such criteria are normally expressed as an upper bound for the load reduction rate measured in each leg, above which more preloading cycles must be performed. In the remainder of this work, for instance, an admissible maximum leg load reduction of 5% in 15 min is adopted as a reference criterion, which is generally representative of the typical jack-up vessels used in the offshore wind industry (and not tied to the specific vessel and/or site conditions described later on).

Some previous studies have contributed to shed light on the relationship between jack-up preloading and time effects in the foundation soil (Le Tirant, 1993; Hedrick and Verret, 2007; Menzies and Roper, 2008; Osborne et al., 2009; InSafeJIP, 2011; Bienen and Cassidy, 2013; Luking et al., 2014; Stanier et al., 2014). General guidance has been provided on how to account for consolidation settlements (i.e., associated with pore pressure dissipation in the soil), and link the preload holding time to permeability/stiffness factors. However, meagre consideration has been so far devoted to viscous time effects, which may be significant in clayey seabeds (Hossain and Randolph, 2009; Versteele et al., 2017).

Field experience about geotechnical time effects has recently led to exploring alternative preloading procedures (Fig. 3), in an attempt to reduce the number of preloading cycles for faster wind farm installation. Versteele et al. (2017) described the strategy illustrated in Fig. 3(a), based on the concept of *overshooting*. Accordingly, the preload target is first exceeded (i.e., *overshot*) to expedite spudcan penetration under the active leg pairs, up to depths that would normally require several cycles of the standard procedure. After overshooting, the leg load is actively reduced to the normal preload target. As discussed later on, this methodology has potential to reduce spudcan settlement occurring in time, so that constant preload can be more easily sustained with limited additional penetration.

Another preloading procedure based on *load-holding* has also been tested in practice – see Fig. 3(b). In this context, the load on the active

legs is first held constant at standard preload target – this is achieved through gradual/controlled leg extension. Afterwards, extension is arrested, and load redistribution is enabled by the delayed settlement that has already begun during the load-holding stage. The process of extending legs to maintain a constant preload is halted when it is expected that the preloading criterion can readily be met.

3. Geotechnical characterisation of the reference site

This study was carried out by considering a specific vessel (Van Oord's *Aeolus* in Fig. 1) operated at a site in the Belgian North Sea. This section overviews relevant geotechnical data obtained from site investigation and laboratory tests – see also Sonnema (2019). This information is summarised hereafter and used in relation to the calibration of a time-sensitive soil constitutive model for 3D FE simulations.

3.1. Analysis of site and laboratory test results

At the reference site location, a shallow clay layer from the Ursel formation (thickness of about 22.7 m) overlies a deeper sand layer. Cone Penetration Test (CPT) data were used to classify different soil layers up to 40 m under the seafloor through Robertson's classification chart (Robertson, 2010). Q_t values were also used to estimate the overconsolidation ratio (OCR) profile in the clay layers, using the empirical relationship proposed by Kulhawy and Mayne (1990): $OCR = 0.32 \cdot Q_t$. The final geotechnical model of the site includes three different soil layers, two clayey and one sandy. CPT-based information was complemented by oedometer laboratory test results to establish the final OCR profile for the clay layers given in Table 1. Overall, the set of available data indicated the presence of significantly over-consolidated clay.

In Fig. 4 distributions of clays' undrained shear strength (s_u) from different sources are compared. In particular, a direct correlation to the

Table 1
Geotechnical parameters for each soil layer at the reference site – down to 40 m depth.

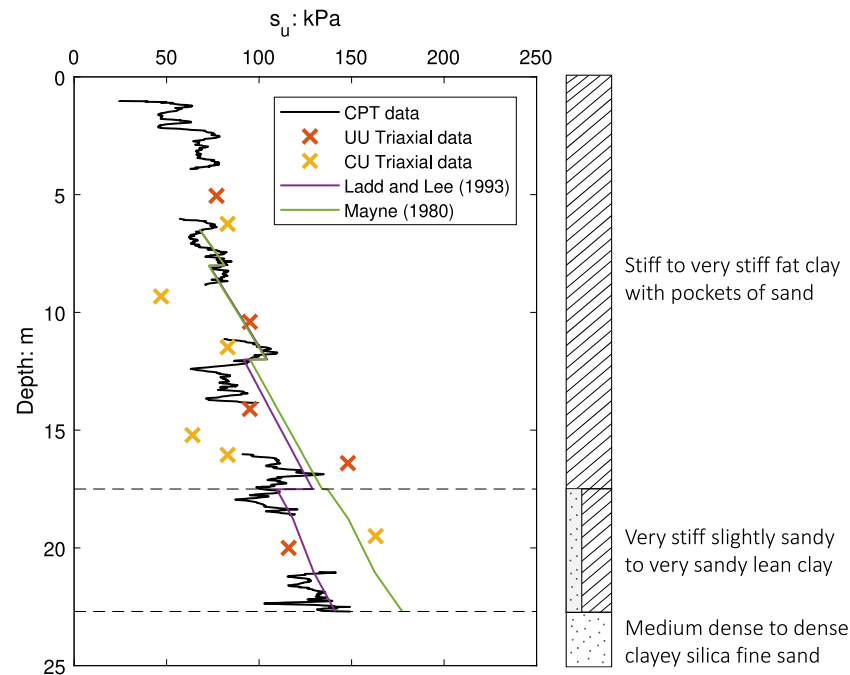| Layer [–]	Depth range [m]	Soil type [–]	γ_{sat} [kN/m³]	OCR [–]	C_c [–]	C_s [–]	E [MPa]	ϕ [deg]	c [kPa]	ψ [deg]
1a	0.0 – 8.0	Clay	18.5	7.0	0.28	0.13	–	30	5	0
1b	8.0 – 12.0	Clay	18.5	6.0	0.28	0.13	–	30	5	0
1c	12.0 – 17.5	Clay	18.5	5.0	0.28	0.13	–	30	5	0
2	17.5 – 22.7	Clay	20.5	4.0	0.21	0.02	–	30	1	0
3	22.7 – 40.0	Sand	19.5	–	–	–	40	40	0	10

Fig. 4. Clay's undrained shear strength values obtained from CPT and laboratory tests results.

CPT profile (black line, $s_u = (q_t - \sigma_v)/N_{kt}$ (Lunne et al., 2002), where $N_{kt} = 26$ was deemed to be appropriate in light of available CU and UU triaxial data) shows visible s_u-jumps at location with drastic variations in OCR. This conclusion is also confirmed when using the empirical correlations by Ladd and Lee (1993) and Mayne (1980). Overall, the s_u profile spans values from 50 kPa to almost 150 kPa, normally associated with stiff, over-consolidated clay. CPT data from the deeper sand layer were translated into indicative friction and dilatancy angles using the empirical relationships by Robertson and Campanella (1983) and Kulhawy and Mayne (1990).

Clay samples extracted from different depths were subjected in the laboratory to oedometer tests, unconsolidated undrained (UU) triaxial tests and consolidated undrained (CU) tests. Fig. 4 shows good agreement between s_u values derived from CPT and triaxial tests. To enable effective stress modelling of clay behaviour, triaxial test results were post-processed in terms of effective stress Mohr's circles to estimate Mohr-Coulomb peak strength parameters (peak friction angle and cohesion) (Muir Wood, 1990).

Since spudcan settlement is largely affected by the compression of the soil underneath (Pisanò et al., 2019), oedometer tests were also executed to investigate the pre-failure stiffness of both clay layers (Fig. 5). Standard compression indices for virgin (C_c) and unloading/reloading (C_s) conditions were derived – see, e.g., Muir Wood (1990) for specific definitions and identification procedures. Fig. 5 reports vertical stress-strain plots (from oedometer tests) and undrained effective stress paths (from CU triaxial tests) for layers 1 and 2. Careful inspection of these experimental results suggested that both clay layers – especially the

shallowest – feature inherently anisotropic behaviour. This conclusion is supported by the high values of the C_s compression index compared to C_c (Fig. 5(a)), as well as by the leftward orientation of the effective stress paths at the onset of deviatoric loading (Graham and Houlsby, 1983) – note the angle between stress paths and vertical direction that is put in evidence in Figs. 5(a) and 5(d).

Table 1 summarises site layering and general effective stress parameters derived for each soil layer (down to 40 m depth) from site/laboratory test results. Relevant soil parameters include: saturated unit weight γ_{sat}, friction angle ϕ, cohesion c, dilatancy angle ψ, and relevant stiffness parameters – C_c and C_s indices for clay, Young's modulus E for sand.[1]

Based on the values of the consolidation coefficient from oedometer test data, soil permeability was evaluated to lie in the range from 10^{-6} to 10^{-8} m/day for clay layer 1 and from 10^{-5} to 10^{-7} m/day for clay layer 2 – depending on the applied confining stress. Real values at the site, however, would be heavily influenced by the severe soil remoulding induced by leg penetration. Therefore, it was preferred to set permeability values based on general recommendations for clayey soils, and then assess the impact of different hydraulic properties through dedicated parametric studies (see Case 4 in Section 5.1). Reference permeability values of 10^{-5} m/day and 10^{-1} m/day were assumed for both clay layers and the underlying sand, respectively.

---

[1] A procedure to estimate the Young's modulus of sands from CPT data is described by Robertson (2009).
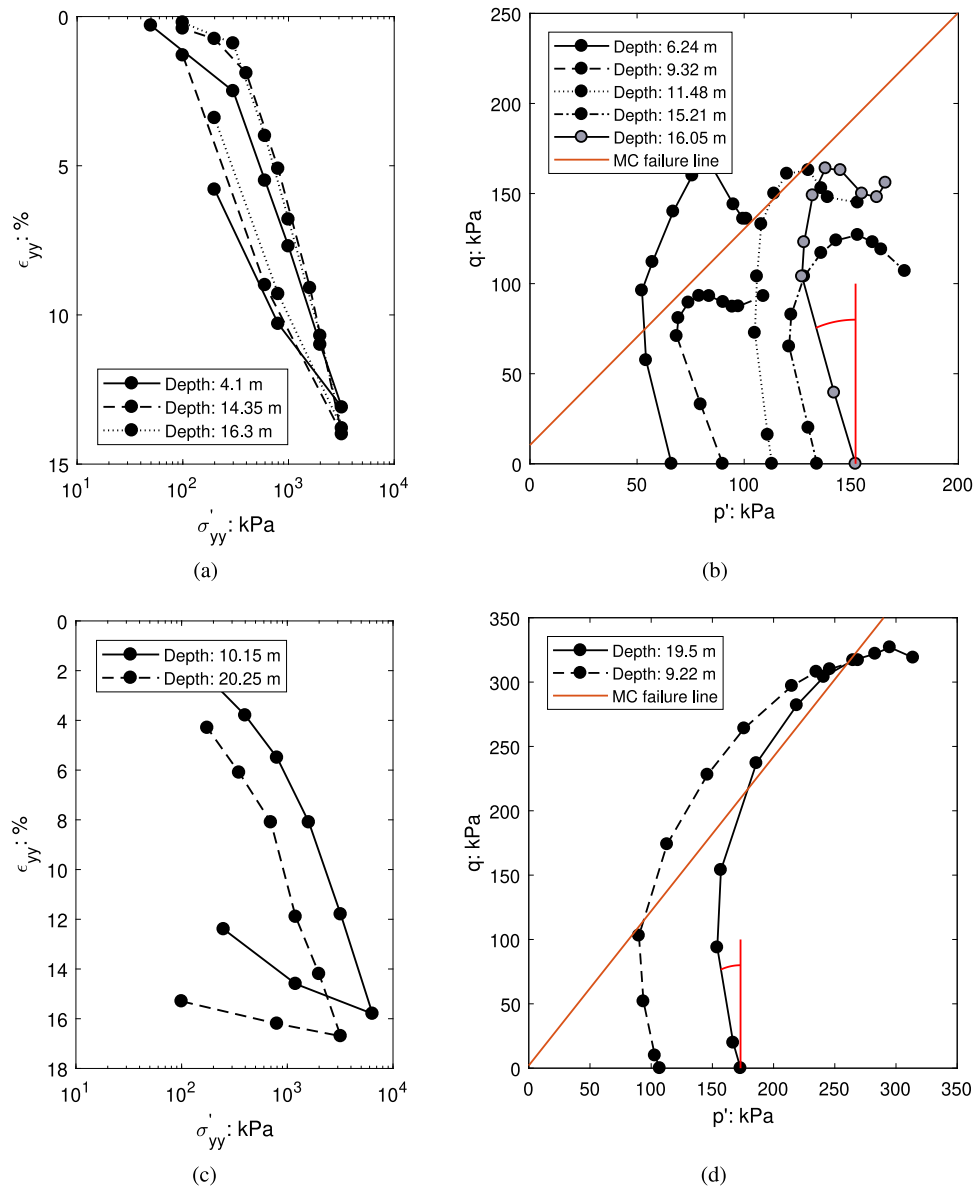
Fig. 5. Representative results of laboratory tests performed on samples from both clay layers. (**a**) Oedometer compression on samples from layer 1 – vertical stress-strain response; (**b**) CU triaxial compression on samples from layer 1 – triaxial effective stress paths; (**c**) oedometer compression on samples from layer 2 – vertical stress-strain response; (**d**) CU triaxial compression on samples from layer 2 – triaxial effective stress paths.

3.2. Plasticity modelling of soil behaviour

The 3D FE analysis of soil–spudcan interaction requires suitable simulation of soil behaviour over a wide range of loading and hydro-mechanical conditions. Herein, the stress-strain response of clayey and sandy soils at the reference site has been modelled via the Soft Soil Creep model and the Hardening Soil Small Strain model, respectively – both available in the PLAXIS 3D FE software (Brinkgreve et al., 2018).

3.2.1. Clay layers

The time-dependent behaviour of clayey soils can markedly affect leg load redistribution during jack-up preloading. Time-dependence emerges from at least two physical mechanisms, i.e., transient interaction between soil skeleton and pore water (soil consolidation), and intrinsically viscous stress-strain behaviour. Different experimental observations may be attributed to the latter, including (i) time-delayed deformation under constant load (creep), (ii) stress relaxation under constant deformation, and (iii) dependence of soil's stiffness/strength on the loading rate (rate-sensitiveness). Particularly, rate-dependence is

most apparent under high strain rates, and therefore usually associated with constant-volume undrained response (Lee and Randolph, 2011). As a consequence, the shear resistance of the soil will be high during initial spudcan penetration, but then will tend to diminish under lower penetration rates as the final depth is approached.

Non-linear viscous effects in soils cannot be reproduced through time-insensitive (also termed 'inviscid') plasticity theories. To overcome this limitation, elasto-viscoplastic constitutive formulations have been devised in the last decades – see the literature reviews provided, e.g., by Sivasithamparam et al. (2015) and Shi et al. (2019). Most elasto-viscoplastic models in the literature assume additive strain decomposition into elastic and irreversible/plastic components. The latter does not follow load application instantaneously, but develops in time depending on the loading rate and specific state variables – hence the term 'visco-plastic'. It is thus possible to unify the modelling of creep, relaxation, and rate-dependence by introducing an irreversible/visco-plastic component of the soil response, while a time-insensitive 'pre-yielding' elasticity is usually retained for simplicity. This approach is especially suitable for normally-consolidated (soft)

Table 2

SSC parameters adopted for the clay layers 1 and 2 at the reference site. For calibration purposes, layer 1 was subdivided into three sub-layers with different OCR values, so as to reasonably match the OCR profile at the reference site (Table 1).

Layer [–]	γ [kN/m³]	e_0 [–]	ν_{ur} [–]	ϕ [deg]	c [kPa]	ψ [deg]	λ^* [–]	κ^* [–]	M [–]	μ^* [–]
1	18.5	0.90	0.3	30	5	0	0.055	0.010	1.65	0.00275
2	20.5	0.65	0.3	30	1	0	0.056	0.011	1.65	0.00275

Table 3

HSS sand parameters adopted for the sand layer at the reference site.

ϕ [deg]	ψ [deg]	E_{50}^{ref} [kPa]	E_{oed}^{ref} [kPa]	E_{ur}^{ref} [kPa]	m [–]	p_{ref} [kPa]	R_f [–]	G_0^{ref} [kPa]	$\gamma_{0.7}$ [–]
40	10	39 000	39 000	117 000	0.5	100	0.92	104 200	$1.35 \cdot 10^{-4}$

clays, since their response is mostly dominated by plastic deformations (due to the initial stress state lying close to the yield locus). Conversely, the same modelling approach will not generate substantial viscous effects for over-consolidated (stiff) clays, due to their response exhibiting prevalent elastic, rate-independent deformations.

In this study, the elasto-viscoplastic Soft Soil Creep (SSC) model was adopted to attempt the simulation of clay's behaviour at the reference North Sea site. The SSC model builds on the work of Vermeer and Neher (1999), who modified the original formulation of the well-known Modified Cam Clay (Roscoe and Burland, 1968) model to include rate-sensitive, visco-plastic strains – an inviscid parent formulation, the Soft Soil (SS) model, is also available in PLAXIS 3D for applications in which time effects are deemed of less importance. The SSC model can capture the abovementioned viscous effects with the same set of parameters, as long as the target experimental evidence is within the reach of the model formulation. The latest version of the SSC model features the following main characteristics (Brinkgreve et al., 2018):

- isotropic elastic response for stress states within the yield locus, with pressure-dependent elastic moduli and constant Poisson's ratio;
- single-hardening cap mechanisms, evolving in presence of volumetric viscoplastic strain increments;
- shear failure occurs when the stress state reaches the Mohr-Coulomb failure envelope. No additional mechanisms to reproduce post-peak strain-softening in OC clay;
- associative plastic flow rule in the cap region, explicitly accounting for the time factor.

The calibration of clay parameters was carried out in three phases – see in Table 2[2] the set of selected parameters for both clay layers:

- the SS parent model was first used to identify effective-stress parameters governing the main features of (elasto-plastic) behaviour, such as virgin and unloading/reloading compressibility, failure friction angle, shape of the yield locus. Figs. 6 and 7 illustrate experiment-model comparisons for oedometer and CU triaxial tests, respectively. Regarding the oedometer unloading/reloading compressibility, it was finally decided not to pursue perfect match of experimental data – the very low C_c/C_s ratio was attributed to soil anisotropy (Table 1), which is a feature of behaviour that the SSC formulation is not suited to reproduce. Conversely, it was preferred to select SSC parameters (λ^* and κ^* in Table 2) more in line with typical values of the C_c/C_s ratio. In addition, priority was given to the primary loading (λ^*) and creep (μ^*) parameters, which mainly determine the (rate of) settlement and other deformation mechanisms;

---

[2] λ^*, κ^*, μ^* denote the (modified) compression, creep, and swelling indeces, respectively.

- the same SS parameters were passed on to the SSC visco-plastic model, while the additional viscous parameter μ^* was calibrated to obtain realistic simulation of rate-dependent undrained strength in CU (consolidated, undrained) triaxial tests (Table 2) – creep test data, whenever available, could also be used to identify μ^*;
- finally, the same tests considered in step (1) were re-simulated using the complete SSC model in combination with loading rates that closely captured real laboratory conditions. In general, this final step may require iterative adjustments to ensure that the parameters identified without accounting for soil viscosity (i.e., using the SS model) would still be appropriate for the elasto-viscoplastic SSC model.

In the lack of specific experimental data, the viscous parameter μ^* in the SSC model was calibrated in step 2 against the following empirical relationship between undrained shear strength (s_u) and deviatoric strain rate ($\dot{\epsilon}_q$) (Einav and Randolph, 2005):

$$\frac{s_u}{s_{u,ref}} = \left[1 + \mu \log \left(\frac{\dot{\epsilon}_q}{\dot{\epsilon}_{ref}} \right) \right] \tag{1}$$

where $s_{u,ref}$ is the reference strength value associated with a reference strain rate $\dot{\epsilon}_{ref}$, while μ is an empirical parameter governing the rate-dependence of s_u. As reported by Hossain and Randolph (2009), $\dot{\epsilon}_{ref}$ and μ lie in the ranges of 1–4 %/h and 0.05–0.2, respectively, for triaxial loading conditions. Fig. 8 shows how the selected SSC parameter μ^* enables, for different initial mean pressure p_0' and OCR, the simulation of rate-dependent s_u trends that are in line with Eq. (1) when low OCR values are considered. In contrast, vanishing rate-dependence results for OCR ≥ 2, due to the simulated material response being predominantly associated with rate-independent elasticity. This behaviour of the SSC model does not fully reflect the experimental evidence regarding the limited impact of OCR on clay's rate-dependence – see, for instance, Zhu and Yin (2000), Sorenson et al. (2007), Lehane et al. (2009), Han et al. (2021) and Hou et al. (2021). Nevertheless, it should be noted that this limitation of the SSC model is shared by the majority of the elasto-viscoplastic formulations for clay presently available in the literature. To practically remedy this shortcoming, the 3D FE studies reported in Section 5 were performed by re-tuning the initial OCR profile to obtain more realistic viscous effects in combination with the other material parameters (which were identified against real site and laboratory data). The choice of a lower OCR in the model may also be regarded as the consequence of the initial leg penetration, i.e., of the increased compression and remoulding of the soil beneath and around the spudcan. Therefore, the initial OCR profile was in essence re-interpreted as an additional modelling parameter – particularly, it was considered that, for the SSC model, OCR values larger than 2 result in negligible creep, whereas unrealistically high creep is typically simulated for OCR < 1.2.

3.2.2. Sand layer

The stiffness of the deeper sand layer was found to only slightly affect soil–spudcan interaction in the considered geotechnical and loading scenarios (Sonnema, 2019). Besides, as viscous effects in sand are known to be far less pronounced than in clay (di Prisco and Imposimato, 1996; Lazari et al., 2019), rate-independent sand behaviour was assumed for simplicity. The Hardening Soil Small Strain (HSS) model provides a well-established platform for modelling the nonlinear monotonic behaviour of sands, including frictional strength, dilatancy, strain-hardening under shear-dominated and compression-dominated loading paths, strain-dependent small strain stiffness (Benz et al., 2009a,b).

In the lack of specific laboratory test results, all HSS parameters were calibrated for a representative relative density $D_r = 65\%$, using the empirical relationships proposed by Brinkgreve et al. (2010). Table 3 reports the full set of calibrated parameters – their role in the HSS model formulation is detailed in Brinkgreve et al. (2018).
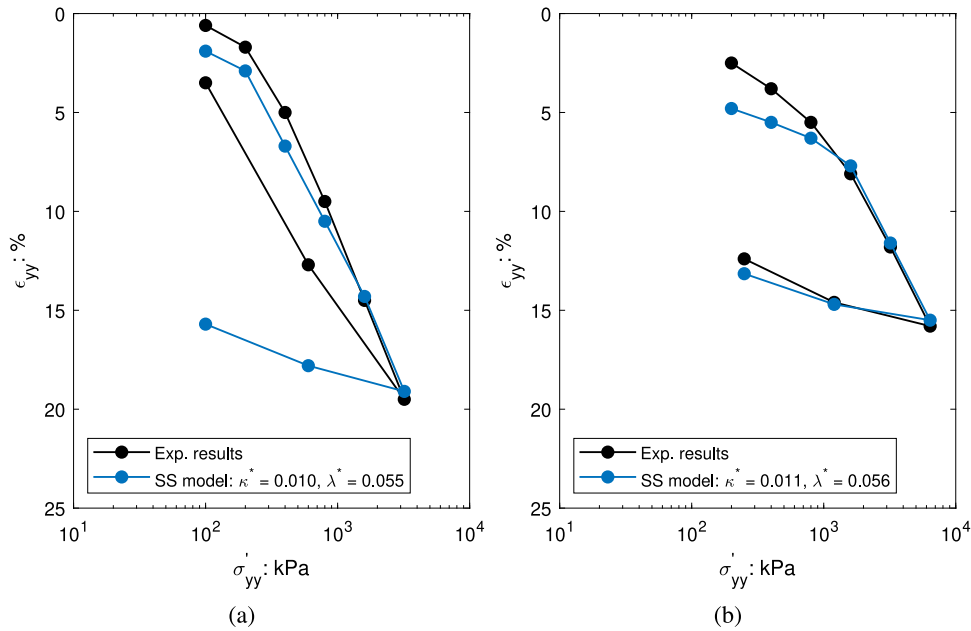
Fig. 6. Calibration of elasto-plastic SSC parameters through SS parent model – oedometer tests: (**a**) clay layer 1; (**b**) clay layer 2.
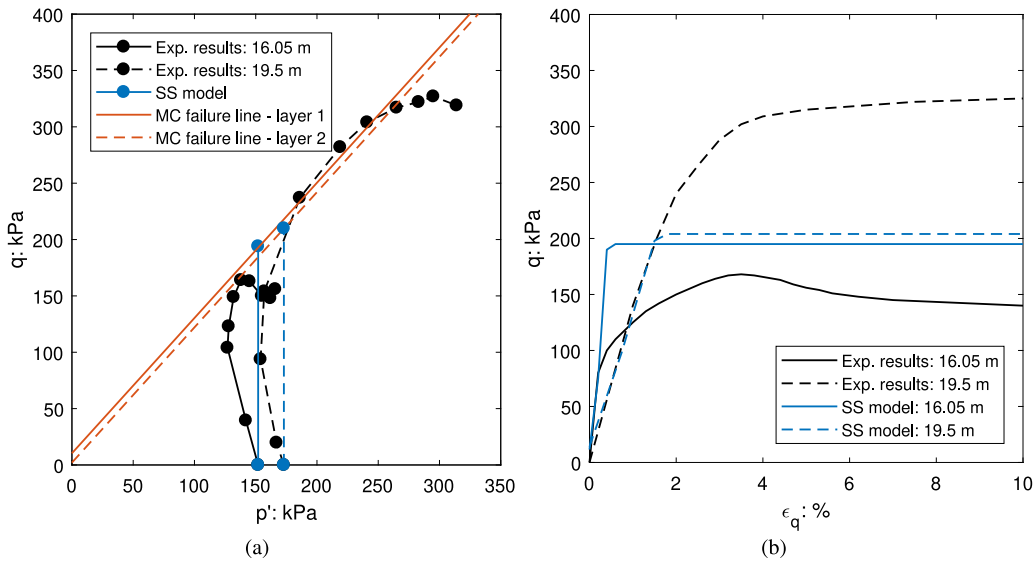

Fig. 7. Calibration of elasto-plastic SSC parameters through the SS parent model – CU triaxial tests: (**a**) stress path; (**b**) deviatoric stress strain response.
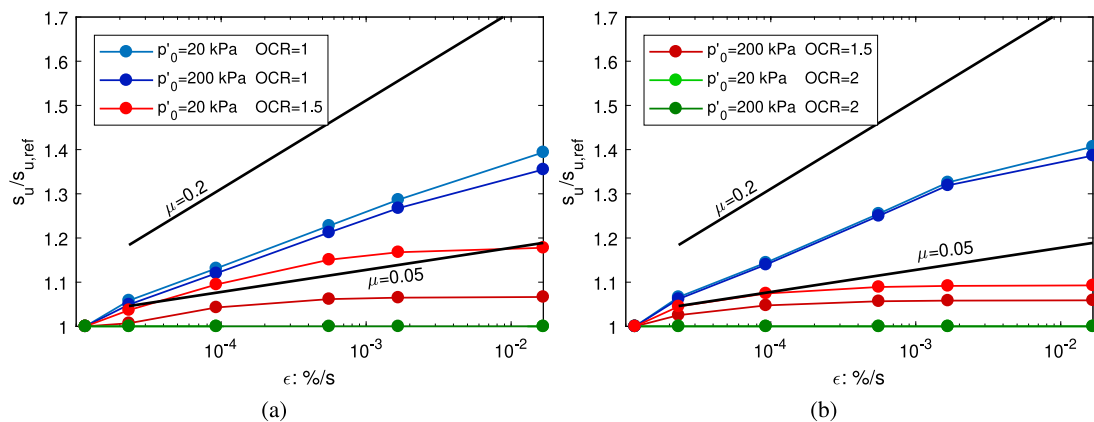

Fig. 8. Simulated rate-dependence of (normalised) undrained shear strength: (**a**) clay layer 1; (**b**) clay layer 2. Comparison between SSC CU triaxial simulations and empirical predictions (black lines) based on Eq. (1). $\dot{\epsilon}_{ref} = 1\%$/h, as proposed by Zhou and Randolph (2007).
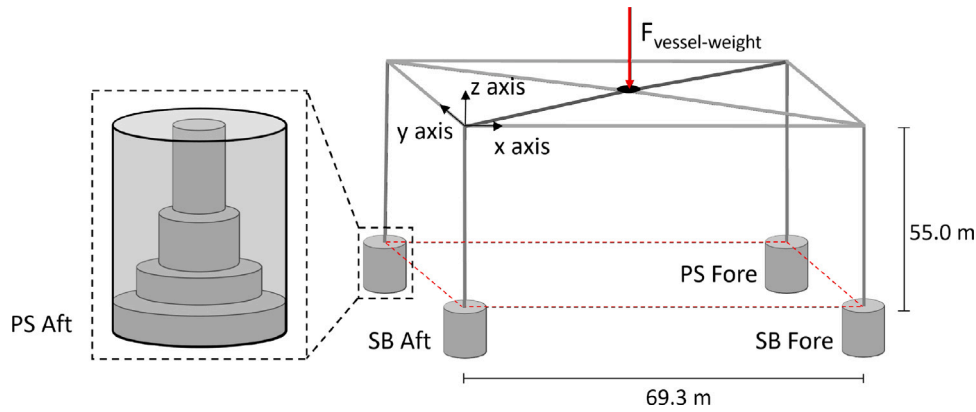
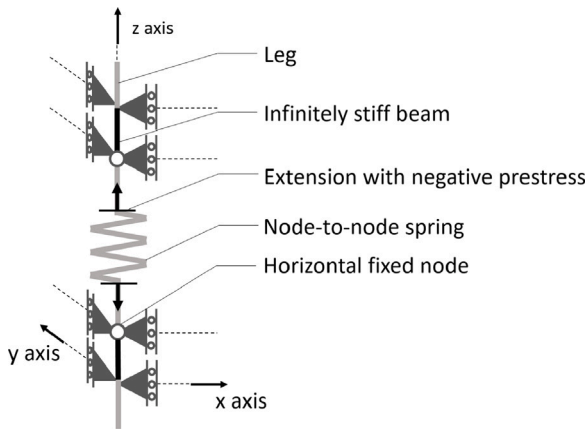**Fig. 9.** Simplified structural model of the jack-up.

Fig. 10. Modelling of the leg extension mechanism during preloading.

Table 4

Geometrical and mechanical properties of the beams used to model the legs and hull of the jack-up. Hull/type 1 and /type 2 beams are shown in light grey and dark grey in Fig. 9, respectively.

Beam type [–]	Material type [–]	E [GPa]	A [m²]	I_x [m⁴]	I_y [m⁴]
Leg	Elastic	210	2.8	3.35	3.35
Hull/Type 1	Elastic	210	2.5	18	18
Hull/Type 2	Elastic	210	2.5	15	15

4. 3D FE modelling of jack-up preloading

This section describes the 3D structural-geotechnical model set up for the *Aeolus* vessel (Fig. 1) using the FE software package PLAXIS 3D (Brinkgreve et al., 2018).

4.1. Jack-up structure

The structural modelling of the considered jack-up includes a simplified geometrical/mechanical representation of the main structural members (hull and legs) and their mutual connections. Specific modelling of the leg extension mechanism was also necessary for the simulation of different preloading procedures.

The flexibility of the hull has prominent influence on internal force redistribution during preloading. A compound beam structure – discretised through 3-node Timoshenko elements (Bathe, 1982) – was assembled to capture the structural flexibility and asymmetry of the hull, as illustrated in Fig. 9. Diagonal hull beams were connected at the centre of gravity, that is 1.5 m nearer to the aft edge than the central mid-axis. The beam properties in Table 4 for the simplified structural model were derived based on a so-called *pre-drive analysis*. Such analysis enabled the identification of equivalent beam properties that closely represented the static response of a more detailed FE model of the vessel – not described herein for brevity. Since weightless beams were adopted in the FE model, the total weight of the structure (with the hull in the air) was applied as an external load (see Fig. 9).

Rigid leg-hull and leg-spudcan connections were assumed, with the four spudcans (being plate-like foundations) and the underground portions of each leg represented as rigid bodies. The spudcan geometry

was further simplified by introducing a flat underside, though with unaltered maximum diameter (see Fig. 9, where the abbreviations SB and PS indicate 'starboard' and 'port-side' footings). Frictional soil–spudcan interfaces were introduced to allow for relative slip; lateral interfaces were extended 1 m under the spudcans' undersides to avoid unrealistically rough contact with the soil at the lowest footing corners. Complete backfill was assumed for spudcan penetration, so that the weight of the soil volume filling the cavity was subtracted from the observed bearing capacity to determine the actual leg load.

So-called 'node-to-node anchors' were adopted to simulate a force-controlled leg extension mechanism. Node-to-node anchors are structural elements representing a spring connection and characterised by their axial stiffness (Brinkgreve et al., 2018). Node-to-node anchors can be extended or contracted by assigning a value of pre-stress, positive/tensile for contraction, negative/compressive for extension.

As shown in Fig. 10, pre-stressed anchors were linked to leg beams through hinged connections. Such connections (i) cannot transmit bending moments, and (ii) need horizontal fixities to prevent loss of equilibrium (Fig. 10). To limit the impact of both issues on the global structural response, the described leg extension mechanism was positioned immediately above the seabed surface. The portion of the leg between the leg extension mechanism and the leg-hull connection was modelled by means of deformable beam elements.

4.2. Soil and spudcan footings

Attention was devoted to adequately discretise the FE soil domain using ten-node tetrahedral elements with four Gauss integration points. After generating soil layers with the above-mentioned properties, five zones of different mesh density were created to more flexibly concentrate elements only where high stress/strain gradients were expected. Such zones are clearly visible in Fig. 11 for an auxiliary 2D/axisymmetric single-spudcan model (footing in grey, soil–spudcan interface lines in green). The following mechanical boundary conditions were set up: total fixity of all nodes on the bottom boundary, prevented horizontal displacement – normal to the boundary – for all side-nodes, and free top soil surface. Free seepage flow through all model boundaries was allowed.
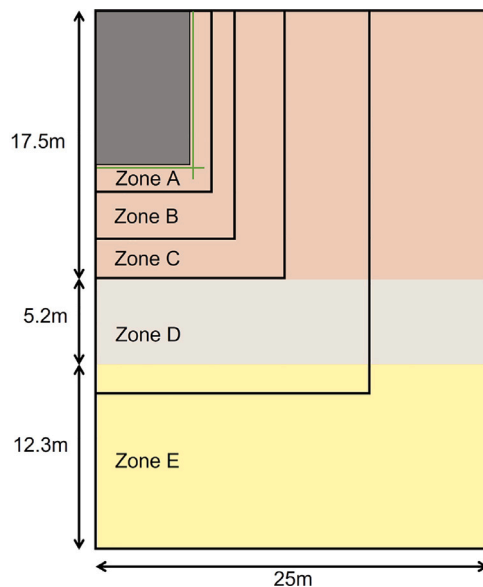
Fig. 11. Zones of different element density in the soil domain (auxiliary 2D model). The green lines indicate the location of foundation-soil interface elements.

Table 5
3D FE analysis programme with different geotechnical/preloading scenarios.

Case	OCR [–]	Clay permeability [m/day]	Preload procedure [–]	Norm. penetration rate [–]
1	2.5 – 4.0	10^{-5}	Standard	0.80
2	1.4	10^{-5}	Standard	0.80
3	1.4	10^{-5}	Standard	0.13
4	1.4	10^{-3}	Standard	0.80
5	1.4	10^{-5}	Overshooting	0.80
6	1.4	10^{-5}	Load-holding	0.80

Convergence trends of numerical solutions were studied at varying element size and density in the soil domain – see Appendix A.1. Preliminary analyses were also carried out to establish optimal soil domain size in combination with the soil parameters in Tables 2–3. Other (unreported) sensitivity analyses were performed to confirm that the side boundaries of the soil model would not affect soil–spudcan interaction (they were placed at a distance of at least 25 m from each leg); as for the bottom sand boundary, 35 m under the seabed was deemed sufficiently deep for the considered spudcan penetration levels. The final 3D FE jack-up–spudcans-soil model is illustrated in Fig. 12.

4.3. FE analysis stages

Performing a complete large-deformation analysis of jack-up installation prior to preloading was beyond the goals of this study. Conversely, the wished-in-place (WIP) approach was followed, with all spudcans initially positioned at the depth reached after the main leg penetration event – after which only moderate soil deformations would be expected. In agreement with field observations, the aft and forward spudcans were placed at initial depths equal to 1.2 and 1.1 times the maximum diameter, respectively. These initial depths were set in consideration both of leg loads and soil bearing capacities – particularly, the larger loads on the aft legs were translated into deeper initial penetrations of the corresponding spudcans. The WIP approach is obviously a drastic simplification of the real installation process, which results in distributions of soil stresses, deformations, and pore pressure that may differ substantially from those returned by complete large-deformation simulations – or by analyses based on the simpler Press-Replace method (Engin et al., 2015; Tehrani et al., 2016). For instance, the initial vertical stiffness of the foundation may not be

entirely representative of the post-penetration interplay between effective stresses and pore pressures around the spudcans. Nevertheless, the simplicity of the WIP approach enabled time-dependent processes and their implications to be studied (at least qualitatively) through less complex/time-consuming simulations.

Each preload analysis was performed according to the following three stages:

– Phase A: generation of initial soil stresses through gravity loading;
– Phase B: application of jack-up's self-weight;
– Phase C: Preloading of opposite leg pairs (first, PS aft + SB forward, then SB aft + PS forward), with soil consolidation phases in between and at the end of the preloading cycle – see Section 5. Real preload values were originally determined in the Site Specific Assessment and then herein normalised (by the maximum value at the considered site) due to data confidentiality.

The mentioned consolidation phases were introduced in the 3D FE analyses to explore how load redistribution is affected by the interaction between pore pressure dissipation and viscous effects in the soil. The numerical analysis of long-lasting soil consolidation was enabled by the use of fully implicit time-integration and large time steps.

Complementary consolidation analyses were also performed using the 2D single-spudcan model in Fig. 11. Their purpose was to clarify how soil consolidation after preloading would affect in time the initial OCR distribution. This aspect appeared immediately relevant in that (i) OCR tends to decrease as external loads are transferred to the soil skeleton around the foundation during consolidation, and (ii) the SSC clay model cannot capture viscous effects for OCR values larger than 2 (see Section 3.2.1).

5. 3D FE simulations of jack-up preloading

The 3D FE model in Fig. 12 was finally employed to analyse six different preloading cases, all conceived as variations of *Aeolus*' real conditions at the site described in Section 3. Specifications for each case are reported in Table 5, including type of preloading procedure, OCR and (assumed) permeability of the soil, average rate of spudcan preloading. Due to data confidentiality, the values of spudcan's initial depth and preloading rate are given in Table 5 after normalisation, respectively by the spudcan diameter and the maximum spudcan penetration rate achieved at the project site (both unspecified for confidentiality). As previously mentioned, different initial penetrations for aft and forward WIP spudcans were set to reflect differences in leg load and soil bearing capacity.

5.1. Qualitative parametric studies

Six preloading cases, including the (pre)loading phase and consolidation phase, were considered to explore how different factors may influence the time evolution of leg loads, and therefore the fulfilment of the aforementioned preloading criterion (i.e., an admissible maximum leg load reduction of 5% in 15 min). In particular, the following situations were taken into account:

– case 1 – soil state and parameters as inferred from site/laboratory data, including realistic OCR distribution along the depth;
– case 2 – uniform distribution of lower OCR, closer to normally consolidated state. This deviation from real site conditions was introduced to emphasise viscous effects as reproduced by the SSC soil model (see Section 3.2.1);
– case 3 – lower preloading rate;
– case 4 – larger clay permeability (sand layer permeability of 0.1 m/day is kept constant);
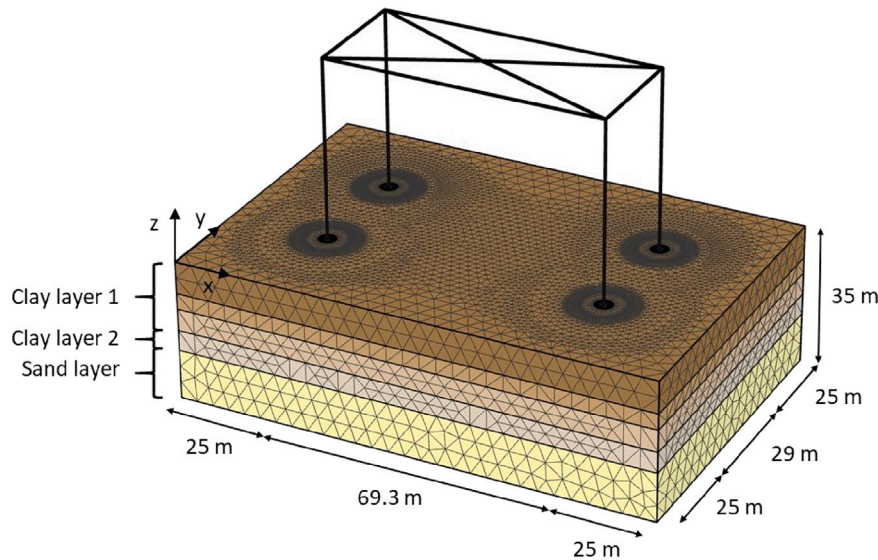– case 5 – alternative preloading procedure, based on *overshooting* (see Section 2);

Fig. 12. Final jack-up–spudcans–soil system 3D FE model.

– case 6 – alternative preloading procedure, based on *load-holding* (see Section 2).

For all cases, numerical results are presented in Figs. 14–19 in terms of (normalised) leg load and spudcan settlement against time for all jack-up legs. Since the leg extension mechanism was modelled as a force-controlled process (see Fig. 10), the resulting spudcan penetration rates cannot be exactly constant. Such rates may be quantified through the slope of the simulated settlement vs time curves.

Distinct analysis stages are numbered in each figure for clarity, while the vertical dashed lines separate consecutive stages. A stage represents a segment of the overall preloading procedure, with a distinction between loading stages (including initial loading as well as the cross-loading of the legs) and holding (i.e., consolidation phase) stages (during which legs hold a fixed position with respect to the hull and loads are monitored against a given preloading criterion). The total number of stages differs for each case and depends on the number of preload cycles. The preload targets and preload criterion for aft and forward legs are represented by distinct red and black dashed lines, respectively, in the left sub-figures.

The results presented in this section show that the factors considered in cases 1 to 6 may in reality impact the timing of soil deformation and associated leg load reduction. Special attention is deserved by the overshooting (case 5) and load-holding (case 6) procedures as possibly effective measures for reducing the number of preloading cycles in the field.

Case 1

Fig. 13 illustrates a cross-section of the soil domain including both aft spudcans. The red area visible in the figure highlights stress points in the soil that are at plastic yielding at the end of the first preload cycle. The asymmetry of the red area around the actively preloaded spudcan indicates significant interaction between footings on the short side of the vessel. The region of influence of each spudcan appears to reach as far as at least one spudcan diameter. Based on Fig. 13, it seems reasonable to conclude that continuum 3D modelling is intrinsically more suitable than lumped macroelements for four-legged jack-ups with near legs – the latter have been most often applied to three-legged drilling units, for which the assumption of non-interacting footings is more applicable (Bienen and Cassidy, 2006).

As expected, Fig. 14 shows only slight load redistribution and spudcan settlements after the preload of both opposite leg pairs – due to different initial spudcan penetrations, preload targets for aft and forward legs are represented by distinct red dashed lines in the left sub-figure. That is a consequence of the relatively large value of the initial OCR in the soil (2.5–4, representative of 'after one day of consolidation'), which hinders the ability of the SSC model to produce significant creep/relaxation. The limited time effects displayed in Fig. 14 are due to (slow) soil consolidation, and would allow the fulfilment of the assumed preloading criterion within one preload cycle.

Case 2

In order to trigger more tangible viscous effects through the SSC model as calibrated in Table 2, a uniform initial OCR equal to 1.4 was set for both clay layers. This corresponds with fictitiously assuming a nearly normally-consolidated state, which however differs from what site data suggested. Considering the limitations of the SSC model, the same distribution of (low) OCR was adopted in all the following cases with the goal of highlighting the interplay between viscous effects and other governing factors – in a fashion that would resemble real time-dependent behaviour in OC clay.

Fig. 15 reports the simulated FE results for a preloading process lasting 1 h and 15 min. Spudcan penetrations upon first preloading equal, respectively, 6% and 7% of the total penetration at the end of the simulation for forward and aft legs. Compared to case 1, however, total penetrations about 30% larger are caused by pronounced delayed deformations in clay – as a consequence of the assumed lower OCR. Within the first preload cycle, the load on the active legs decreases by approximately 6%, which is not compatible with the aforementioned preloading criterion.

These observations can be easily justified from a constitutive modelling perspective. When OCR ≈ 1, viscous effects are emphasised by stress states lying closer to the yield locus in the soil around each footing. Starting from a low over-consolidation ratio (namely, OCR = 1.4), active preloading tends to further reduce such a slight over-consolidation, and therefore increase the rate of delayed creep/relaxation. As load levels are higher in active legs than in the passive pair, faster time evolution of leg loads in the former is also unsurprisingly found.

Multiple preload cycles are needed in case 2 to fulfil the preloading criterion. Active leg load reduction is about 6.4% and 5% in the first and second cycles, respectively. Although this supports the validity of repeating preloading operations, two preloading cycles per leg are necessary in this case to achieve acceptably low leg load reduction. It is also important to remark the quantitative relevance of the initial OCR distribution – as shown by the comparison between case 1 and case 2
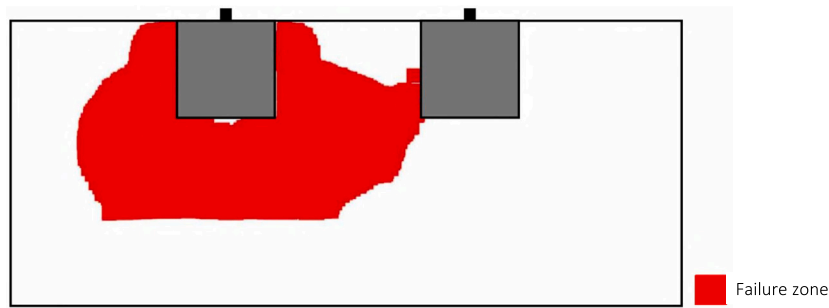
Fig. 13. Plastic points distribution after first preload cycle.
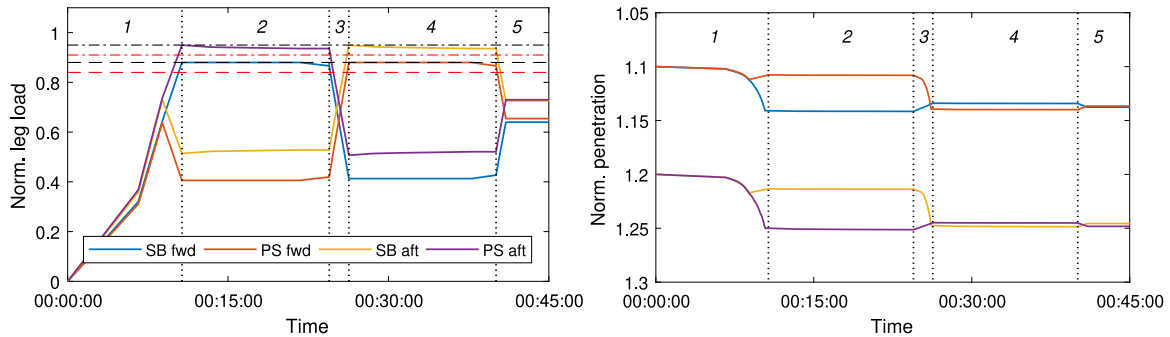

Fig. 14. Simulation results for case 1 – total duration: 45 min. The normalised initial spudcan depth is 1.1 and 1.2 for the forward and aft spudcans respectively. The preload targets and preload criterion for aft and forward legs are represented by distinct red and black dashed lines.
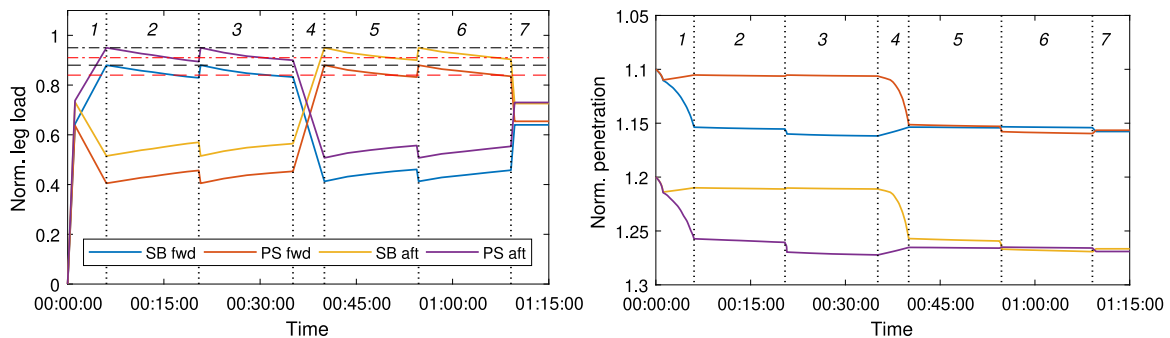

Fig. 15. Simulation results for case 2 – total duration: 1 h and 15 min.

(in which different initial OCR are considered). Noting again that the adopted elasto-viscoplastic modelling framework would not produce significant viscous effects for OCR values larger than 2, it was preferred in the following four cases to retain the same OCR distribution assumed in case 2. As previously mentioned, this choice corresponds with regarding the initial OCR profile as a sort of additional modelling parameter.

Case 3

The normalised penetration rate was then decreased from 0.8 to 0.13 (values normalised with respect to the largest penetration rate observed at the site) – see the corresponding 3D FE results in Fig. 16. Numerical results for case 3 show spudcan penetration approximately 10% larger than in case 2 at the end of the first preload cycle (stage 4 in the figure), but with subsequent leg load reduction of only 4.4% – it is around 6% in case 2. In addition to creep/relaxation effects, viscous soil behaviour also implies sensitiveness to loading rate – usually with higher resistance associated with larger loading rate. As the SSC model can actually capture this aspect in nearly normally-consolidated clays, it is not surprising to find deeper spudcan settlement under slower loading. In the after-loading phase, however, less viscous resistance is

mobilised during slower penetration, which leads to lower settlement than under faster preloading (case 2). Overall, these differences compensate each other, so that very similar total settlements are obtained in cases 2 and 3. As the preloading criterion is fulfilled after four preload cycles both in cases 2 and 3, the latter turns out to take more time (more than two hours) due to the lower spudcan penetration rate – see Fig. 16.

Case 4

The results in Fig. 17 illustrate the role of clay's permeability, which was increased here from 10^{-5} m/day to 10^{-3} m/day while preserving the same loading programme as in case 2. 3D FE simulation results indicate that, due to faster soil consolidation, larger/faster spudcan settlement and leg load reduction take place in this case. In more detail, leg load reduction in the first preload cycle is approximately 8.4%, and 7% in the second. The preloading criterion is not yet met after two preload cycles, so that more cycles and longer preloading time are required. Overall, the results in Fig. 17 are not too far from those obtained for Case 2, due to the soil response remaining nearly undrained despite the larger permeability.
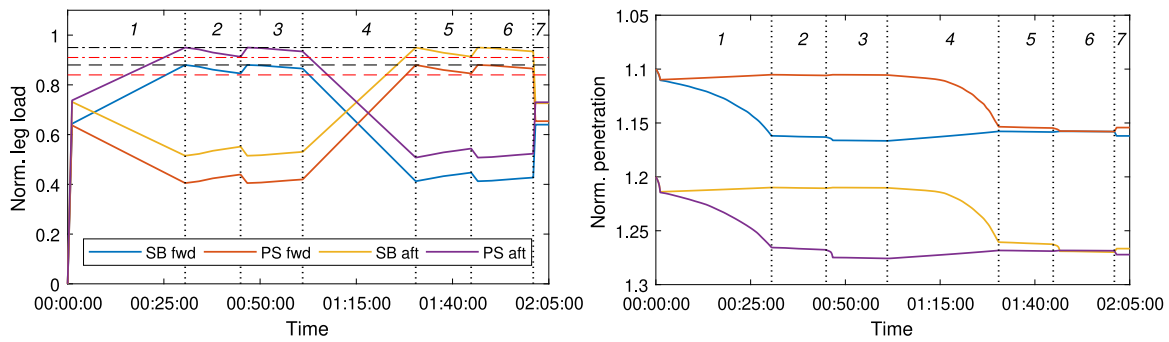
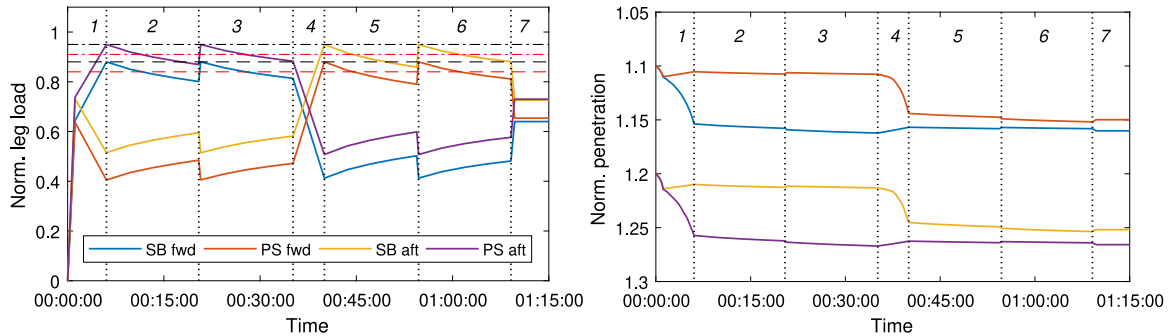**Fig. 16.** Simulation results for case 3 – total duration: 2 h and 5 min.

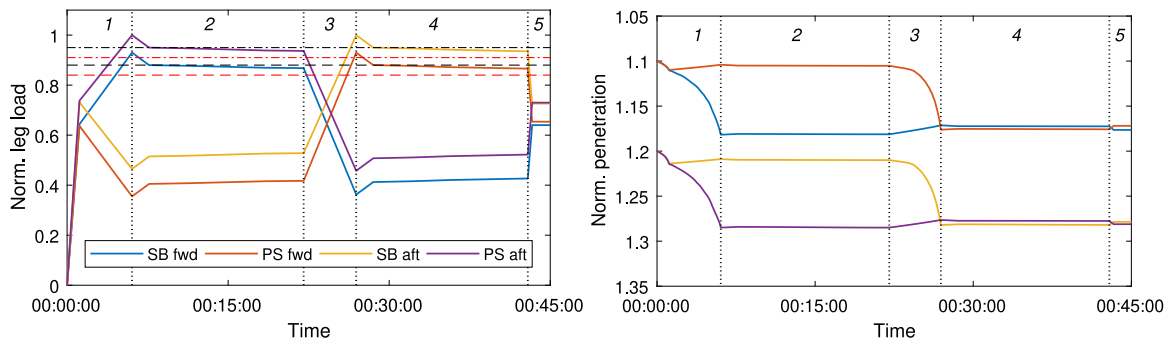**Fig. 17.** Simulation results for case 4 – total duration: 1 h and 15 min.

Fig. 18. Simulation results for case 5 – total duration: 45 min.

Case 5

The 3D FE results in Fig. 18 allow a preliminary evaluation of the overshooting procedure as described in Section 2. The first active leg pair was loaded beyond the established preload target (whence the term *overshooting*), then the load level was actively reduced to such target before allowing for consolidation/creep settlements in the soil. The overshot value of the normalised preload target in case 5 was increased to a value of 1.0 and 0.95 for the aft and forward legs, respectively, which is 5% larger than the preload target considered in all previous cases. It is interesting to observe that the preloading criterion is readily met during the first preload cycle – the leg load reduces by only 1% during the whole consolidation phase. The results in Fig. 18 indicate that, in this specific case, the overshooting procedure may be more effective than standard preloading in reducing the total preloading time. From a geotechnical standpoint, the success of the overshooting procedure relates to the earlier penetration of the active spudcans, down to depths that would only be reached after delayed deformations. It is thus natural to expect that less room is left for further settlement – and therefore load redistribution – when the consolidation/viscous phase begins.

Case 6

The second alternative procedure described in Section 2 builds on the idea of holding the load constant for some time after achieving the standard preload target (*load-holding procedure*). Fig. 19 shows that the active legs penetrate only very slightly while the preload target is held constant (phases 2 and 5). Following nearly linear load reductions during consolidation phases, a total decrease of 4.6% results, for instance, at the end of phase 3. Such reduction is slightly lower than that observed during the second preload cycle in case 2 (Fig. 15). Although the resulting improvement is relatively small and a second preload cycle is still required, the considered load-holding procedure shows some potential for the mitigation of leg load reduction in comparison to the standard preloading procedure.

5.2. Comparison to real jacking data

Despite the acknowledged limitations of the 3D FE model, a final attempt was made to benchmark, at least qualitatively, its performance against real jacking data. After generating the initial stress field in the 3D FE model, the vessel load was applied prior to simulating the considered preloading cases, in order to obtain through the model the
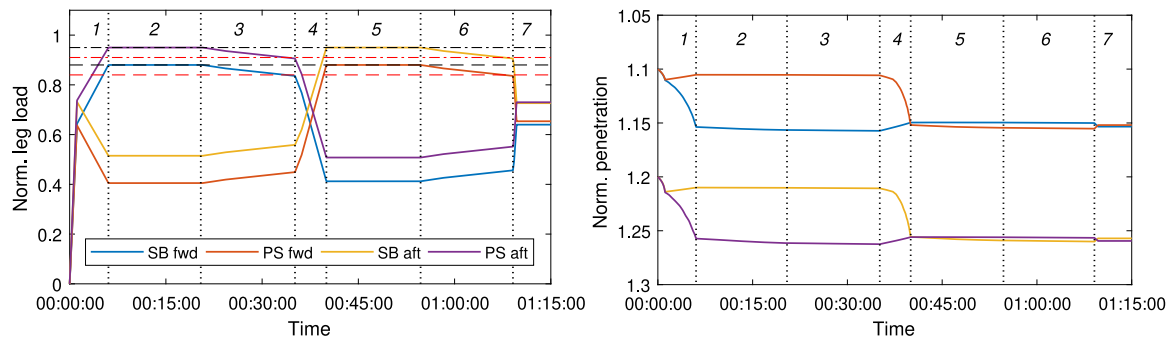
Fig. 19. Simulation results for case 6 – total duration: 1 h and 15 min.
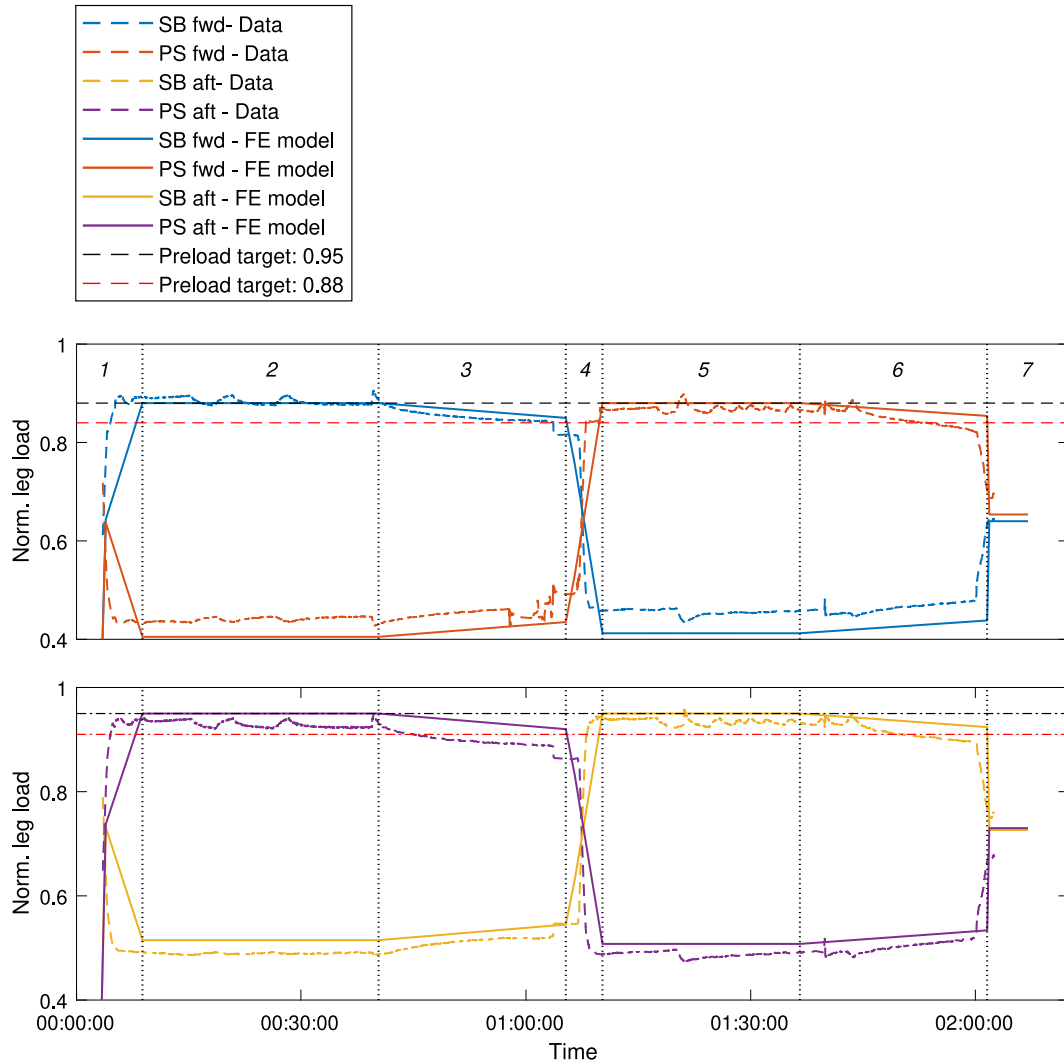

Fig. 20. Time evolution of measured and simulated leg loads.

initial leg penetration and the corresponding stress redistribution in the soil. Figs. 20 and 21 show the evolution in time of the leg load and the spudcan settlement as emerging from measured data (dashed lines) and numerical simulations (solid lines). Data and simulation results regarding the aft and forward legs are shown in separate sub-plots.

The reference preloading sequence for the considered load level took place over approximately two hours, with about one hour preloading time for each leg pair. Consolidation/viscous settlement phases of about 25 min were allowed for each leg pair. The number of preloading cycles cannot be precisely established for field measurements, as legs

are frequently extended. Through frequent leg extension it was possible to keep the load on the active legs at its target value, while 6% load reduction was recorded for both the aft and forward legs due to delayed soil settlement during the consolidation/viscous phase. During this phase (stages 3 and 6 in the figures), about 50% of the total load reduction occurred in the first five minutes, then significantly lower reduction rate was observed (only 10% load reduction in the last ten minutes).

Numerical 3D FE results were obtained using the following model settings and assumptions:
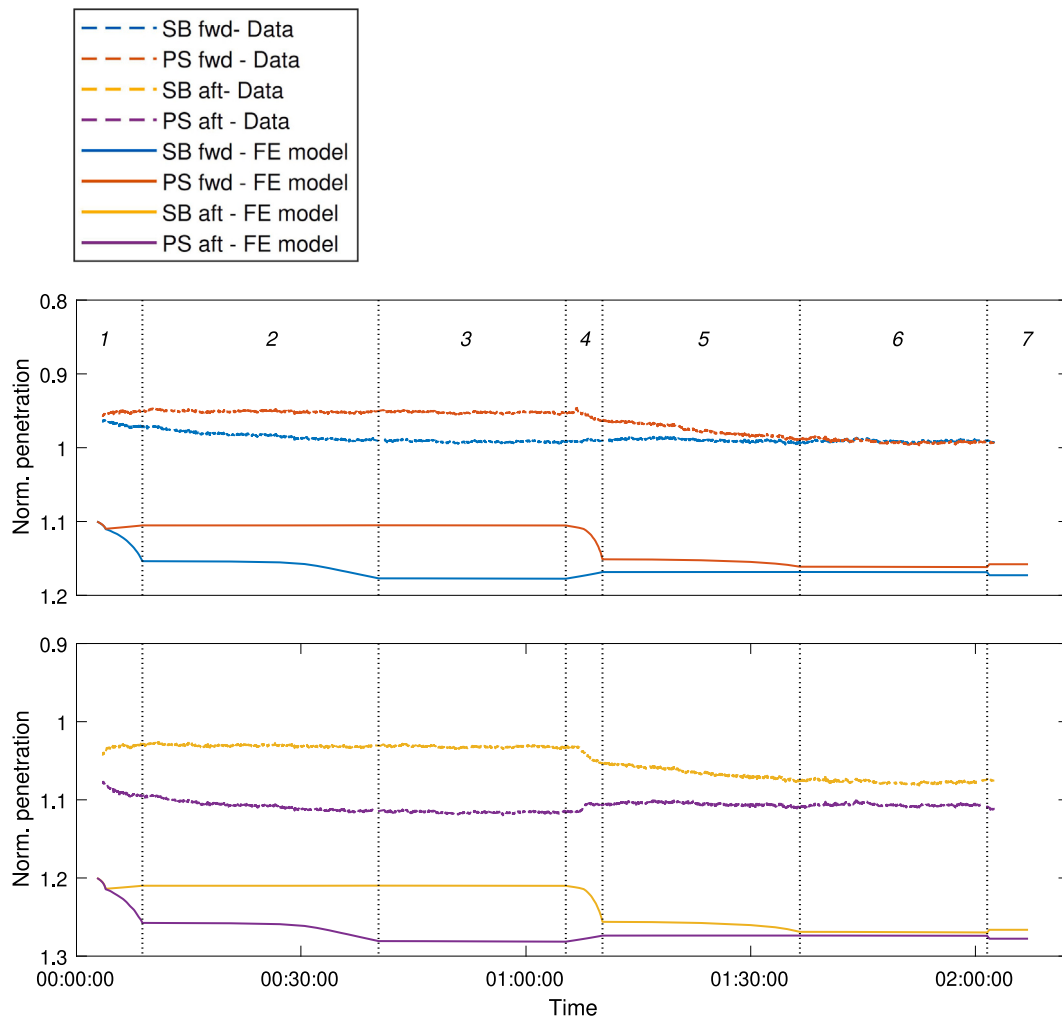
Fig. 21. Time evolution of measured and simulated leg penetrations.

- initial OCR equal to 1.4 for both clay layers, and assumed permeability of 10^{-5} m/day;
- normalised leg penetration equal to 1.1 and 1.2 for forward and aft legs, respectively;
- imposed preloading rate consistent with field measurements;

The reported 3D FE results reasonably capture the most relevant aspects of the recorded preloading response, including the time patterns of leg-load redistribution that determine the fulfilment of the considered preloading criteria. As for spudcans' settlement, jacking in the field led to final normalised penetrations of approximately 1.0 and 1.1 for the forward and aft legs, respectively (Fig. 21). In agreement with load-time trends, it can be observed how the active legs were continually extended to preserve the load target, with negligible penetration of the passive spudcans. When active preloading was switched to the other leg pair (stage 4), penetration and uplift occurred for the 'new' active and passive spudcans, respectively. Although not fully comparable to field data, the 3D FE model provides sound results also in terms of footing settlement and related time effects. Relevant settlement and uplift stages are well captured for all spudcans, including the time-delayed deformations associated with soil consolidation and creep.

In the attempt to include creep effects by setting OCR = 1.4 in the SSC model, the amount of creep may have been overestimated. This could be concluded from the (too) high rate of penetration simulated during preloading (phases 1 and 4). At the same time, the (undrained) shear strength may also have been underestimated (Fig. 4), thereby

leading to the generation of excessive plastic deformations. The latter is more likely to be the reason for the overestimated settlement rate.

After numerically simulating the same preloading programme as in the field, 3D FE results indicate that the adopted preloading criterion is met at the end of the second cycle (stage 6). Although this conclusion is not fully accurate when compared to measured data, it still possible to conclude that the 3D FE model returns results that are in qualitative agreement with field observations. As for the differences in initial spudcan penetration between the 3D FE model and the measured data, they may be the natural outcome of the abovementioned limitations of the numerical model, including the crude idealisation of laterally homogeneous soil across the site.

6. Discussion

The simplified Wished-In-Place (WIP) was adopted in this research to generate the initial location of the spudcan after leg penetration, i.e., by disregarding the real large-deformation process and associated soil remoulding. While the intended focus of this study is on the interaction between time effects in the soil and jack-up preloading scheme, the mentioned limitation has led to a necessary re-interpretion/re-calibration of relevant soil parameters with respect to the information available from site investigation and laboratory data. In particular, the analysis of soil creep through the SSC model is highly dependent on the OCR input – the model does not reproduce any soil viscosity for highly over-consolidated clays, which were abundant at the considered site.

Table 6
Mesh setups considered in the preliminary mesh sensitivity study.

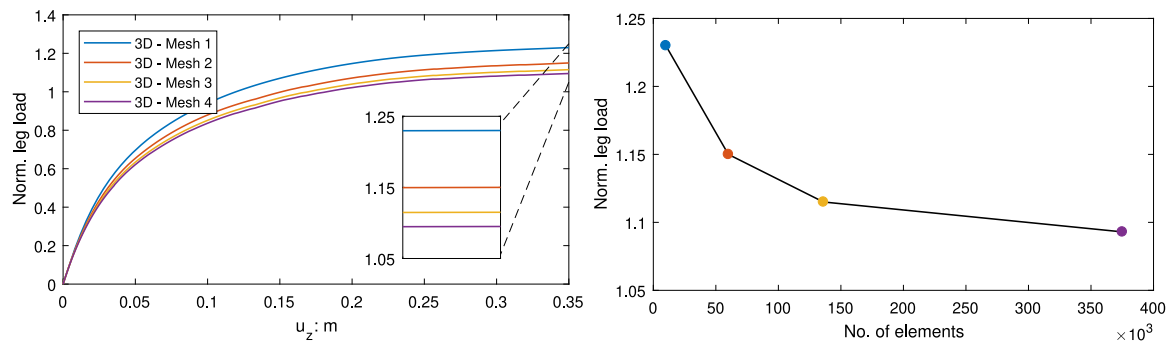| Mesh no.	No. of elements	Average element size [m]					Max norm. leg load
		Zone A	Zone B	Zone C	Zone D	Zone E	
1	14 499	0.5	0.7	1.9	3.1	3.7	1.23
2	69 228	0.3	0.5	1.0	2.9	3.7	1.15
3	134 672	0.2	0.5	0.5	2.9	3.7	1.12
4	369 350	0.15	0.35	0.5	2.9	3.7	1.09

Fig. 22. FE results from the mesh sensitivity study.

Therefore, this intrinsic limitation of the available constitutive model was artificially overcome by setting an OCR profile characterised by values lower than foreseen in reality. On the other hand, the set-up of a lower OCR in the model may also be regarded as the consequence of the initial leg penetration, i.e., of the increased compression and remoulding of the soil beneath and around the spudcan.

Time effects in the considered boundary value problem arise from the complex interplay of soil creep, rate-sensitivity, and consolidation – all affected by the external loading rate. Within the timeframe considered in the above analyses, some consolidation (dissipation of pore pressures) was observed, which in turn had to have an impact on creep deformations through the underlying variation of the OCR. From the comparison to real jacking data it could be concluded that the amount of creep may have been overestimated, which could be concluded from the excessively high spudcan penetration rate during preloading (phases 1 and 4) – also a possible consequence of underestimated undrained shear strength values.

Further to the intrinsic limitations of its viscoplastic formulation, the SSC model also disregards the influence of clay anisotropy. In fact, the oedometer test data available for soil samples from the project site showed, for the clay layer 1, values of the unloading/reloading compression stiffness similar to those obtained under primary loading stiffness – an anomaly possibly related to the soil anisotropy pointed out in Section 3. Since the SSC model does not allow for high values of both stiffness parameters, it was chosen to pursue best agreement for the primary compression stiffness – and therefore to accept the underestimation of soil rebound effects upon unloading.

7. Concluding remarks

An integrated, wished-in-place 3D FE model was set up to analyse preloading operations on four-legged jack-ups in clay, and particularly delayed spudcan settlements and leg load redistribution caused by soil consolidation and viscosity. For model development purposes, real data concerning Van Oord's Aeolus jack-up at a Belgian North Sea site were considered. The availability of detailed geotechnical data allowed to calibrate the Soft Soil Creep viscoplastic model available in PLAXIS 3D. However, engineering judgement had to be used to calibrate the parameters governing soil permeability and viscosity – due to lack of relevant experimental information.

After the setup and verification of the numerical model, parametric studies were performed to investigate the influence of several governing factors, such as clay's permeability and OCR, preloading rate and sequence. All the parameters considered proved influential, in that they can affect the timing of soil deformation and associated leg load redistribution. Ultimately, the fulfilment of an assumed preloading criterion has a strong, case-specific dependence on the rate of soil–structure interaction. These considerations motivated the analysis of two alternative preloading procedures, based on the concepts of *overshooting* and *load-holding*. Numerical results indicated that both procedures possess good potential for reducing the number of preloading cycles, and therefore the total jack-up installation time (and related costs).

Overall, the results presented in this study support the suitability of 3D FE modelling as a tool for the Site Specific Assessment of jack-up preloading. Fully satisfactory results may hardly be achieved through lumped soil-foundation modelling, due to limited mutual distances among spudcans in small four-legged jack-ups. The accuracy of 3D FE predictions, however, is markedly affected by the capability of the adopted constitutive model to reproduce the real behaviour of marine soils. Existing knowledge gaps include, for instance, the modelling of time effects and anisotropy in over-consolidated clay, as well as the inclusion of large deformations and remoulding arising from initial leg penetration. Further research and comparisons to field data will be necessary in the future for advanced 3D modelling to provide reliable quantitative support to Site Specific Assessments.

CRediT authorship contribution statement

Wouter Sonnema: Conceptualization, Methodology, Software, Formal analysis, Data curation, Writing – original draft, Writing – review & editing. **Sanne Brinkman:** Conceptualization, Methodology, Supervision, Writing – review & editing. **Ronald B.J. Brinkgreve:** Conceptualization, Methodology, Supervision, Writing – review & editing. **Federico Pisanò:** Conceptualization, Methodology, Supervision, Writing – original draft, Writing – review & editing.

Declaration of competing interest

The authors declare that they have no known competing financial interests or personal relationships that could have appeared to influence the work reported in this paper.

Data availability

The data that has been used is confidential

Acknowledgements

Appendix

A.1. Space discretisation of the soil domain

Preliminary FE bearing capacity calculations were performed to establish appropriate element size and distribution within the soil domain. In particular, the case of a single spudcan wished in place 10 m under the seabed was considered, with the soil modelled as a homogeneous Tresca material (total stress undrained analysis) for simplicity. The soil domain around the spudcan was modelled as 3D box with dimensions equal to 50 m × 50 m × 35 m (length × width × depth). As previously mentioned, five mesh zones with different element size/density were defined to optimise the computational costs – see Fig. 11. Table 6 reports for meshes 1 (coarsest) to 4 (finest) the total number of elements, and the average element size within the five mesh zones, from A to E. Mesh refinement was mostly applied to the soil mass in the vicinity of the spudcan, where most intense stress/strain gradients are expected to arise during loading.

The results of the mesh sensitivity study are reported in Fig. 22 in terms of load-displacement response (left) and maximum foundation capacity against total number of elements (right). Fig. 22 (right) shows very clearly a converging trend as finer meshes are considered. As a trade-off between good accuracy and bearable computational burden, mesh 3 was finally selected (mesh 4 would have been returned very similar results in a longer time). The final model with four spudcans in Fig. 12 was built by introducing element size zones similar to those reported in Table 6.

References

Andersen, K., 2015. Cyclic soil parameters for offshore foundation design. In: The 3rd McClelland Lecture.

Barbosa-Cruz, E.R., 2007. Partial Consolidation and Breakthrough of Shallow Foundations in Soft Soil (Ph.D. thesis). The University of Western Australia, Australia.

Bathe, K.-J., 1982. Finite Element Procedures in Engineering Analysis. Prentice-Hall.

Benz, T., Schwab, R., Vermeer, P., 2009a. Small-strain stiffness in geotechnical analyses. Bautechnik 86 (S1), 16–27.

Benz, T., Vermeer, P., Schwab, R., 2009b. A small-strain overlay model. Int. J. Numer. Anal. Methods Geomech. 33 (1), 25–44.

Bienen, B., Cassidy, M.J., 2006. Advances in the three-dimensional fluid-structure-soil interaction analysis of offshore jack-up structures. Mar. Struct. 19 (1), 110–140.

Bienen, B., Cassidy, M.J., 2013. Set up and resulting punch-through risk of jackup spudcans during installation. J. Geotech. Geoenviron. Eng. 139 (12), 2048–2059.

Bienen, B., Ragni, R., Cassidy, M.J., Stanier, S.A., 2015. Effects of consolidation under a penetrating footing in carbonate silty clay. J. Geotech. Geoenviron. Eng. 141 (9), 04015040.

Brinkgreve, R., 2004. Time-dependent behaviour of soft soils during embankment construction - a numerical study. In: Pande, G., Pietruszczak, S. (Eds.), Numerical Models in Geomechanics. CRC Press / Balkema - Taylor and Francis Group, pp. 631–637.

Brinkgreve, R., Engin, E., Engin, H., 2010. Validation of empirical formulas to derive model parameters for sands. In: Numerical Methods in Geotechnical Engineering. CRC Press, pp. 153–158.

Brinkgreve, R.B.J., Kumarswamy, S., Swolfs, W.M., Foria, F., 2018. PLAXIS 3D User Manual. PLAXIS B.V.

Dean, E.T.R., 2010. Offshore Geotechnical Engineering: Principles and Practice. ICE Publishing.

di Prisco, C., Imposimato, S., 1996. Time dependent mechanical behaviour of loose sands. Mech. Cohes.-Frict. Mater. 1 (1), 45–73.

Einav, I., Randolph, M.F., 2005. Combining upper bound and strain path methods for evaluating penetration resistance. Internat. J. Numer. Methods Engrg. 63 (14), 1991–2016.

Engin, H., Brinkgreve, R., Van Tol, A., 2015. Simplified numerical modelling of pile penetration–the press-replace technique. Int. J. Numer. Anal. Methods Geomech. 39 (15), 1713–1734.

Engin, H.K., Jostad, H., D'Ignazio, M., Sivasithamparam, N., Huynh, D.V.K., Andersen, K., Johansson, J., Kaynia, A., Torgersrud, O., Yetginer, G., Hofstede, H., 2019. Advanced site-specific analysis of skirted spudcans in the view of north sea experiences. In: International Conference: The Jack-Up Platform Design, Construction & Operation.

Globaldata, 2012. Healthy Competition: Demand Grows for Specialised Offshore Vessels. World Expo.

Graham, J., Houlsby, G.T., 1983. Anisotropic elasticity of a natural clay. Géotechnique 33 (2), 165–180.

Han, J., Yin, Z.Y., Dano, C., Hicher, P.Y., 2021. Cyclic and creep combination effects on the long-term undrained behavior of overconsolidated clay. Acta Geotech. 16, 1027–1041.

Hedrick, W.P., Verret, S.M., 2007. Jackup operations: new operational recommended practices. In: Proceedings of Offshore Technology Conference, OTC 18980, Houston, Texas.

Hossain, M.S., Randolph, M.F., 2009. Effect of strain rate and strain softening on the penetration resistance of spudcan foundations on clay. Int. J. Geomech. 9 (3), 122–132.

Hou, Y., Zhou, Y., Zhao, B., Li, G., 2021. Experiments of creep rate for over-consolidated clay under plain strain condition and a simple correlation. All Earth 33, 88–97.

Houlsby, G., 2016. Interactions in offshore foundation design. Géotechnique 66 (10), 791–825.

Hoyle, M., Stiff, J., Hunt, R., Morandi, A., et al., 2006. Jack-up assessment-past, present and ISO. In: The Sixteenth International Offshore and Polar Engineering Conference. International Society of Offshore and Polar Engineers.

InSafeJIP, 2011. Improved Guidelines for the Prediction of Geotechnical Performance of Spudcan Foundations During Installation and Removal of Jack-Up Units. Joint Industry Funded Project.

ISO, 2016. ISO 19905-1 Petroleum and Natural Gas Industries - Site-Specific Assessment of Mobile Offshore Units - Part 1: Jack-Ups. Technical Report, International Organization for Standardization.

Jiang, Z., 2021. Installation of offshore wind turbines: A technical review. Renew. Sustain. Energy Rev. 139, 110576.

Kulhawy, F.H., Mayne, P.H., 1990. Manual on Estimating Soil Properties for Foundation Design. Report EL 6800, Electric Power Research Institute.

Ladd, C.C., Lee, S., 1993. Engineering Properties of Sergipe Clay: Tps Progress Report No. 4. Technical Report. Research Report R93-07, Department of Civil and Environmental Engineering, MIT.

Lazari, M., Sanavia, L., di Prisco, C., Pisanò, F., 2019. Predictive potential of perzyna viscoplastic modelling for granular geomaterials. Int. J. Numer. Anal. Methods Geomech. 43 (2), 544–567.

Le Tirant, P., 1993. Design Guides for Offshore Structures. Technip Editions.

Lee, J., Randolph, M., 2011. Penetrometer-based assessment of spudcan penetration resistance. J. Geotech. Geoenviron. Eng. 137 (6), 587–596.

Lehane, B.M., O'Loughlin, C.D., Gaudin, C., Randolph, M.F., 2009. Rate effects on penetrometer resistance in kaolin. Géotechnique 59 (1), 41–52.

Luking, J., Wenzel, S., Martens, L., 2014. Modelling installation and construction of offshore wind farms. In: 33rd International Conference on Ocean, Offshore and Arctic Engineering, OMAE. pp. 1–12.

Lunne, T., Powell, J.J., Robertson, P.K., 2002. Cone Penetration Testing in Geotechnical Practice. CRC Press.

Mayne, P.W., 1980. Cam-clay predictions of undrained strength. J. Geotech. Eng. Divis. 106, 1219–1242.

Menzies, D., Roper, R., 2008. Comparison of jackup rig spudcan penetration methods in clay. In: Proceedings of Offshore Technology Conference, OTC 19545, Houston, Texas.

Muir Wood, D., 1990. Soil Behaviour and Critical State Soil Mechanics. Cambridge University Press.

Osborne, J., Bienen, B., Cassidy, M.J., Randolph, M.F., 2009. Improved guidelines for the prediction of geotechnical performance of spudcan foundations during installation and removal of jack-up units. In: Proceedings of Offshore Technology Conference, OTC 20291, Houston, Texas.

Pisanò, F., Schipper, R., Schreppers, G.-J., 2019. Input of fully 3D FE soil-structure modelling to the operational analysis of jack-up structures. Mar. Struct. 63, 269–288.

Ragni, R., Bienen, B., Wang, D., Mašín, D., Cassidy, M.J., 2017. Numerical modelling of the effects of consolidation on the undrained spudcan capacity under combined loading in silty clay. Comput. Geotech. 86, 33–51.

Ragni, R., Wang, D., Mašín, D., Cassid, M., Stanier, S., 2016. Numerical modelling of the effects of consolidation on jack-up spudcan penetration. Comput. Geotech. 78, 25–37.

Randolph, M.F., Gourvenec, S., 2011. Offshore Geotechnical Engineering. Spon Press.

Robertson, P.K., 2009. Interpretation of cone penetration tests - a unified aproach. Can. Geotech. J. 46, 1337–1355.

Robertson, P.K., 2010. Soil behaviour type from the CPT: an update. In: 2nd International Symposium on Cone Penetration Testing, CPT'10.

Robertson, P.K., Campanella, R.G., 1983. Interpretation of cone penetration tests. Part I: Sand. Can. Geotech. J. 20 (4), 718–733.

Roscoe, K., Burland, J., 1968. On the generalized stress-strain behavior of wet clays. Proc. Eng. Plast. 535–609.

Shi, Z., Hambleton, J.P., Buscarnera, G., 2019. Bounding surface elasto-viscoplasticity: A general constitutive framework for rate-dependent geomaterials. J. Eng. Mech. 145 (3), 04019002.

Sivasithamparam, N., Karstunen, M., Bonnier, P., 2015. Modelling creep behaviour of anisotropic soft soils. Comput. Geotech. 69, 46–57.

SNAME, 2008. Guidelines for Site Specific Assessment of Mobile Jack-Up Units. Technical and Research Bulletin 5-5A Rev. 3, Society of Naval Architechts and Marine Engineers.

Sonnema, W., 2019. 3D FE Analysis of Four Legged Jack-Up Vessels During Preloading in Cohesive Soil (Master's thesis). Delft University of Technology, Netherlands, URL: https://repository.tudelft.nl/.

Sorenson, K.K., Baudet, B.A., Simpson, B., 2007. Influence of structure on time-dependent behaviour of a stiff sedimentary clay. Géotechnique 1, 113–124.

Stanier, S.A., Ragni, R., Bienen, B., Cassidy, M.J., 2014. Observing the effects of sustained loading on spudcan footings in clay. Géotechnique 64 (11), 918–926.

Tehrani, F.S., Nguyen, P., Brinkgreve, R.B.J., van Tol, A.F., 2016. Comparison of press-replace method and material point method for analysis of jacked piles. Comput. Geotech. 78, 38–53.

Vermeer, P.A., Neher, H.P., 1999. A soft soil model that accounts for creep. In: Proc. Int. Symp. beyond 2000 in Computational Geotechnics - 10 Years of PLAXIS International. pp. 249–261.

Versteele, H., Cathie, D.N., Kuo, M.Y.K., 2017. Planning the preloading procedure to account for rate-effects in clays. In: International Conference: The Jack-Up Platform, London.

Wang, D., Bienen, B., 2016. Numerical investigation of penetration of a large-diameter footing into normally consolidated kaolin clay with a consolidation phase. Géotechnique 66, 1–6.

Welaya, Y.M., Elhewy, A., Hegazy, M., 2015. Investigation of jack-up leg extension for deep water operations. Int. J. Nav. Archit. Ocean Eng. 7 (2), 288–300.

Zhou, H., Randolph, M.F., 2007. Computational techniques and shear band development for cylindrical and spherical penetrometers in strain-softening in clay. Int. J. Geomech. 7 (4), 287–295.

Zhu, J., Yin, J., 2000. Strain rate-dependent stress-strain behavior of overconsolidated hong kong marine clay. Can. Geotech. J. 37 (6), 1272–1282.